Irregularity and Locking to the Seasonal Cycle in an ENSO Prediction Model as Explained by the Quasi-Periodicity Route to Chaos

ELI TZIPERMAN

Atmospheric and Oceanic Sciences Program, Princeton University, Princeton, New Jersey

MARK A. CANE AND STEPHEN E. ZEBIAK

Lamont-Doherty Earth Observatory, Columbia University, Palisades, New York

(Manuscript received 15 March 1994, in final form 14 June 1994)

ABSTRACT

The behavior of the Cane–Zebiak ENSO prediction model is analyzed as a function of model parameters measuring the strength of coupling between the model ocean and atmosphere and the amplitude of the background seasonal cycle specified in the model. As either of these two parameters is increased, the model undergoes a transition from periodic to chaotic behavior according to the universal quasi-periodicity route to chaos. Thus, the irregularity of model ENSO events and their partial locking to the seasonal cycle can both be explained as low-order chaotic behavior driven by the seasonal cycle. The chaos is due to irregular jumping of the Pacific natural ocean–atmosphere oscillator between different nonlinear resonances with the seasonal forcing.

The periodic seasonal forcing seems to be the main factor determining the chaotic behavior of the model. However, the full irregularity of model ENSO events is only explained by considering additional factors, possibly including the nonlinear interaction of different delay oscillator modes related to the different model ocean Rossby modes.

1. Introduction

Recent work on the mechanisms of the El Niño–Southern Oscillation (ENSO) has significantly advanced our understanding of ENSO dynamics. The body of work using various simple delay oscillator models has provided quite a satisfactory explanation for the onset, termination, and cyclic nature of ENSO events (Suarez and Schopf 1988; Graham and White 1988; Battisti and Hirst 1989; Cane et al. 1990; Munnich et al. 1991). Neelin et al. (1994) review the state of ENSO theory, including extensions to the delay oscillator physics and work using various fuller ENSO models. Two basic ENSO characteristics unexplained by the delay oscillator mechanism are the irregular occurrence of ENSO events and their apparent partial locking to the seasonal cycle (Rasmusson and Carpenter 1982).

ENSO's irregularity was suggested by Graham and White (1988) to be the result of random forcing due, for example, to atmospheric weather. Such "random" forcing might be high-order chaotic behavior of the ocean–atmosphere system due to deterministic dynamical processes that are characterized by timescales much shorter than ENSO's and that are external to the basic ENSO mechanism. An alternative explanation for ENSO's irregularity was given by Vallis (1986, 1988) and Munnich et al. (1991), both suggesting that the irregularity is not a result of an external random force but instead is due to the inherent nonlinearity of the ENSO system, resulting in a low-order chaotic behavior. While Vallis (1986, 1988) has used an ENSO model that lacks the equatorial wave dynamics now accepted as a crucial factor of ENSO dynamics, Munnich et al. (1991) have used a nonlinear delay oscillator model to show that irregular, and seemingly chaotic, motion may occur without an explicit external noise term.

The partial locking of ENSO to the seasonal cycle, seemingly contradicting its irregularity, was attributed to various factors. Zebiak and Cane (1987) suggested that it might be due to a seasonal dependence of the strength of the coupling between ocean and atmosphere. Vallis (1988), although using a model that lacks the essential equatorial wave dynamics, has shown that with nonlinear dynamics and simple seasonal forcing, one might obtain a locking of the system's response to the annual forcing frequency.

Recently, Tziperman et al. (1994, hereafter T94) and Jin et al. (1994) have proposed that ENSO behavior is consistent with low-order chaotic behavior driven by

Corresponding author address: Dr. Eli Tziperman, Environmental Science and Energy Research, Weizmann Institute of Science, Rehovot 76100, Israel.

the seasonal cycle. It was found that the resulting chaotic behavior may provide a simple explanation for both the irregularity of ENSO events and their locking to the seasonal cycle. Chaos arises because the natural oscillator of the equatorial Pacific coupled ocean–atmosphere system can enter into nonlinear resonance with the seasonal cycle at several periods of the oscillator (mostly 2–5 years). The coexistence ("overlapping") of these resonances results in chaotic behavior due to the irregular jumping of the system between the different resonances. In particular, it was shown by T94 using a simple delay model and by Jin et al. (1994) using a simplified coupled model, that as the nonlinearity of the delay model is increased, the system's transition from simple periodic behavior to chaotic behavior is according to the so-called quasi-periodicity route to chaos (Bohr et al. 1984; Jensen et al. 1984; Bak et al. 1985: all three works hereafter referred to as BBJ84] and follows the universal behavior of this class of chaotic systems.

While the idea of ENSO as a seasonally driven chaos seems quite appealing, one would like to see it demonstrated using a more complete model than those used in T94 and in Jin et al. (1994). This is the purpose of the present manuscript. We show here that the same basic chaos mechanism that was demonstrated in T94 using a highly simplified delay model is also at work in the ENSO prediction model of Zebiak and Cane (1987) (hereafter the CZ model). This more realistic model allows some important refinements and corrections to the original ideas derived using simpler models.

In the following sections we first describe the universal properties of the quasi-periodicity route to chaos using the simplest model system that undergoes this route to chaos: the circle map (section 2). Some aspects of the CZ model relevant to the numerical experiments carried out in this work are described in section 3. The diagnostic tools used to analyze the transition to chaos of the CZ model are explained in section 4, and the numerical experiments demonstrating this transition scenario in the CZ model are given in section 5. We conclude in section 6.

2. Quasi-periodicity route to chaos, the circle map

The transition to chaos of a model system as its nonlinearity is increased can occur in one of several standard scenarios. The main ones are the period doubling route, the intermittency route, and the quasi-periodicity route to chaos, which will be shown to be the one relevant here. Each of these transition scenarios has several universal properties common to all physical systems undergoing it.

The quasi-periodicity route to chaos occurs in periodically forced nonlinear physical systems. The simplest model system for this scenario is the circle map, which is an iterative map of the circle to itself. The model equation is

$$\theta_{n+1} = f_\Omega(\theta_n) = \theta_n + \Omega - \frac{K}{2\pi}\sin(2\pi\theta_n), \quad (1)$$

where θ_n is the angle denoting the location of the nth iteration on the circle, taken modulo 1 in this equation. The circle map is nonlinear, with the nonlinearity measured by the parameter K. The quasi-periodicity route to chaos is a two-parameter route; that is, both the nonlinearity parameter K and Ω are varied to obtain the full behavior of the transition to chaos.

The circle map has been investigated in detail, as were other simple physical systems undergoing the same route to chaos, and there is a wealth of universal properties of the quasi-periodicity route to chaos that are now well understood (BBJ84). We will describe only those properties essential for the following discussion of the transition to chaos of the CZ ENSO model and refer the reader to the references for additional details.

An important parameter in diagnosing the transition to chaos of the circle map is the "winding number" ω. It is the mean number of rotations around the circle per iteration of the map (1). If, for example, $\omega = 0.5$, then θ_n will require two iterations to complete a 360 degree trajectory. For the circle map, the winding number is defined as the limit

$$\omega = \lim_{N\to\infty} \frac{1}{N}(\theta_N - \theta_0), \quad (2)$$

where θ_N is not taken modulo 1 for this calculation. For a more general physical system the winding number is calculated in a slightly different way that is described and demonstrated in the following sections.

Consider first Fig. 1 [based on Fig. 9 of Bak et al. (1985)], schematically showing the transition of the circle map to chaos as function of the two parameters K and Ω. The wedgelike areas beginning as a single point on the horizontal axis and widening as K increases are known as "Arnol'd tongues." These tongues are areas in which the winding number ω is a rational number (given by the starting point of the tongues on the horizontal axis), and the solution for θ_n is perfectly periodic. There is an infinite number of such Arnol'd tongues, and only the main ones are shown in the figure. These areas represent regions in which the solution is in a state of nonlinear resonance. Note that while a linear resonance occurs when the internal frequency of the system equals that of the external forcing, a nonlinear resonance may occur when the ratio of the two frequencies is a rational number P/Q. The strong main resonances are characterized by small P and Q (e.g., $\omega = 1/4$), while the weaker secondary resonances are those with larger P and Q (e.g., $\omega = 3/10$). Each of the two tongues P/Q and P'/Q' gives rise to a next level tongue characterized by the ratio $(P + P')/(Q + Q')$. The two largest tongues are at $P/Q = 0/1$ and $P/Q = 1/1$. Hence, the second level consists of the tongue $(0 + 1)/(1 + 1) = 1/2$, the next level

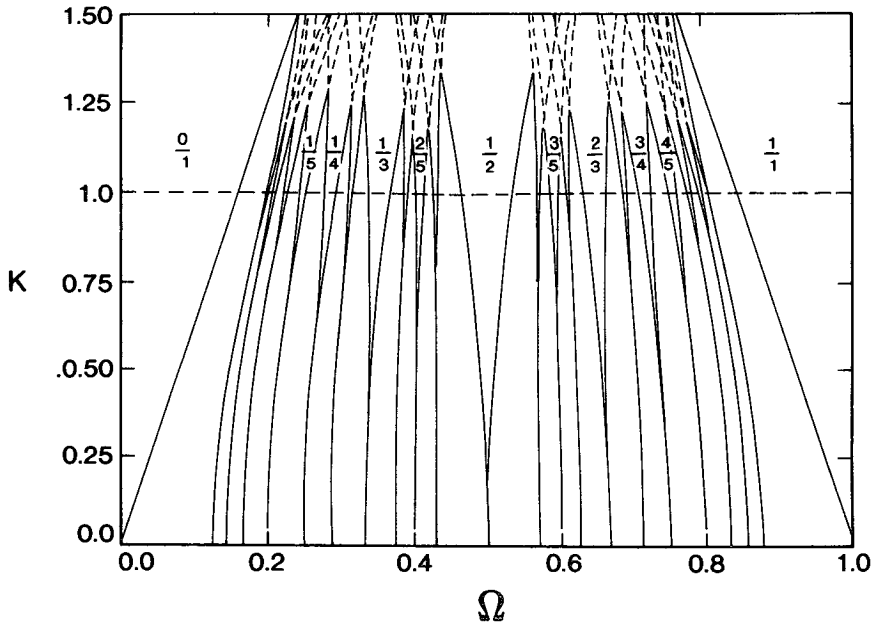

FIG. 1. Schematic phase diagram for the circle map, based on Fig. 9 of Bak et al. (1985). The main nonlinear resonances (Arnol'd tongues) are shown, and their overlapping in the chaotic regime is seen above $K = 1$.

includes 1/3 and 2/3, and the next one consists of the four tongues at 1/4, 2/5, 3/5, and 3/4.

The transition of the circle map to chaos as the nonlinearity is increased occurs as follows. For small nonlinearity K most of the solutions are not in nonlinear resonance but are simply quasi-periodic; that is, the map's winding number ω is not a simple rational number.

For larger nonlinearity, the Arnol'd tongues cover a larger part of the Ω axis. At $K = 1$ they cover nearly the entire axis, so that the total length of all the intervals that are not within the Arnol'd tongues is of measure zero (zero total length), and practically all Ω values result in mode-locked behavior.

For $K > 1$, some of the Arnol'd tongues overlap. (Figure 1 shows only the main resonances, and these overlap only above the line $K = 1$.) When this occurs, several nonlinear resonant solutions are possible for a single choice of the parameters Ω and K. The system, now "frustrated" (BBJ84) by its inability to decide which resonance to settle on, jumps irregularly between the possible resonances. Between jumps, the system still tends to be locked to the external frequency for some interval of time. In the regime in which the 1/3 tongue overlaps that of the 1/4, for example, the time series will not be completely random but will have distinct segments in which its frequency (i.e., the winding number) is 1/4 and others in which it is 1/3.

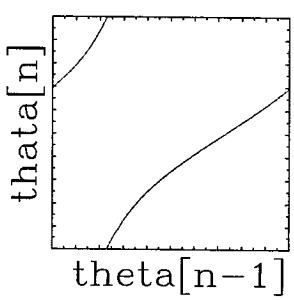

FIG. 2. The return map for the circle map.

A useful diagnostics of the transition to chaos of the circle map is the "return map" of θ_n versus θ_{n-1} that is shown in Fig. 2 for the quasi-periodic regime where it is a monotonically increasing function. The transition to chaos occurs at $K = 1$ when the monotonicity is lost and $\partial\theta_n/\partial\theta_{n-1} = 0$ at some point. For more complex physical systems, the return map develops "wrinkles" at the transition to chaos (BBJ84).

We now proceed to describe the ENSO model used here, and then examine its transition to chaos in the light of the universal properties of the quasi-periodicity transition to chaos described above for the circle map.

3. The model and relevant parameters

The version of the CZ model used here was described by Zebiak and Cane (1987, section 4c). The model state that is judged "optimal" in terms of fitting to the observed ENSO characteristics was analyzed in T94 and found to be consistent with a low-order chaotic

behavior. This conclusion was based on a calculation of the Grassberger–Procaccia correlation dimension from a model time series (Grassberger and Procaccia 1983). The correlation dimension was used to distinguish between the two possible explanations for the irregularity of the ENSO model time series: low-order chaos (characterized by a low value for the correlation dimension) and random noise (large correlation dimension). However, it is difficult to differentiate low-order chaos from random noise using time series analysis alone. While all known precautions were taken in estimating the correlation dimension in T94, a final verification that the CZ model is indeed governed by a low-order chaotic process requires more than a low estimate for the correlation dimension.

In order to demonstrate that the irregularity of ENSO events in the CZ model results from a chaotic behavior, we need to explore the model behavior as some of its parameters are changed beyond the physically realistic regime. Two model parameters are varied in this study: the strength of the drag coefficient relating wind velocity to wind stress and the amplitude of the background seasonal cycle. Given the wind velocity in the model, $\mathbf{u}_a = (u_a, v_a)$, the stress acting on the ocean (τ_x, τ_y) is given by

$$(\tau_x, \tau_y) = \rho_{\text{air}} r_d C_d |\mathbf{u}_a| (u_a, v_a), \qquad (3)$$

where C_d is the drag coefficient and ρ_{air} is the air density, assumed constant. The drag coefficient C_d may be regarded as a factor determining the strength of the coupling between the ocean and the atmosphere in this model (Cane et al. 1990). As it is reduced below some critical level, the coupled instability responsible for the ENSO events in the model is eliminated and the model solution stops oscillating. The parameter r_d is a relative drag coefficient that is equal to 1 in the standard model configuration and is varied in the experiments below.

The CZ model has five specified background fields that are meant to reflect the climatological state of the Pacific Ocean and atmosphere. There are the climatological monthly SST, ocean surface currents, upwelling velocity, surface winds, and surface wind divergence. These fields are specified in the model as monthly values at each horizontal grid point in the model. Let $F^{\text{model}}_{i,j,l}$ denote any of the specified model background fields at a horizontal location (i, j) and month l. In order to vary the seasonal amplitude of the background fields specified in the model, we write

$$F^{\text{model}}_{i,j,l} = \bar{F}^{\text{data}}_{i,j} + a_{\text{seasonal}}(F^{\text{data}}_{i,j,l} - \bar{F}^{\text{data}}_{i,j}), \qquad (4)$$

where $F^{\text{model}}_{i,j,l}$ is the background field used in the model run, $F^{\text{data}}_{i,j,l}$ represents the actual Pacific monthly climatology (e.g., the climatological monthly SST), and $\bar{F}^{\text{data}}_{i,j}$ is a time-independent Pacific climatology taken in our experiments to be either the July climatology or the annual mean climatology. The parameter a_{seasonal} specifies the amplitude of the seasonal cycle. When it is equal to 1, the background monthly state used by the model is equal to the actual Pacific climatology. When a_{seasonal} is zero, the background state reduces to the time-independent climatology $\bar{F}^{\text{data}}_{i,j}$. In all the experiments described below, the amplitude of the seasonal cycle is varied uniformly for all five background fields specified in the CZ model.

4. Diagnostics used to examine model time series

The analysis of the transition to chaos of the CZ model is done in this work by running the model with various parameter values and examining the model NINO3 time series (averaged sea surface temperature over the model's East Pacific: 5°S–5°N, 90°–150°W). The model time series is obtained by running the CZ model for 100 years to dissipate the transient response to the model initial conditions, and then 1024 more years in which the NINO3 time series is saved for later analysis. The elimination of transients turns out to be crucial. A model state that may seem irregular at the beginning of a run, for example, could settle on a perfectly periodic solution after a while.

In this section we briefly describe the diagnostics we have used to examine time series from the CZ model and characterize its chaotic behavior.

a. Reconstructed phase space

The phase space coordinates for a collection of particles are simply the location and velocity of all particles. Given a time series from a complex observational or model system, the concept of particle trajectories is not always usable, but a "reconstructed" phase space picture may be obtained by using "delay coordinates." Let the time series be $h(t)$. Then, an equivalent m-dimensional phase space picture is obtained by using the delay coordinates

$$\mathbf{h}(t) = [h(t), h(t + \tau), h(t + 2\tau), \cdots, h(t + (m - 1)\tau)]. \qquad (5)$$

These delay coordinates can be shown to provide a picture equivalent to the actual phase space picture for the system from which the time series is taken. The delay time τ is normally chosen to be the decorrelation time for the time series $h(t)$, although sometimes more elaborate ways are needed to maximize the information content of the phase space picture (Fraser and Swinney 1986). We have used $\tau = 1$ year. Note that the delay time or delay coordinates are not related to the delay oscillator concept for the ENSO system. For the quasi-periodicity route to chaos, a two-dimensional phase space picture ($m = 2$) is sufficient to extract the information about the transition to chaos.

b. Power spectrum

The power spectrum of a model time series may be most illuminating when examining the transition to

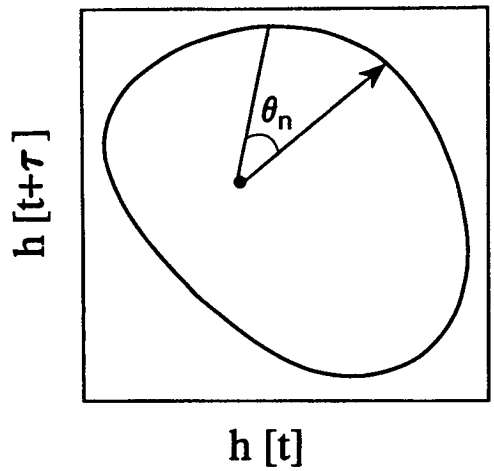

FIG. 3. Calculating the return map from a general quasi-periodic time series.

chaos of a nonlinear system. In the nonchaotic regime, the spectrum is characterized by several very sharp peaks, while in the chaotic regime, the spectral peaks become fewer and wider. To calculate the spectrum, we have used routine G13CBF from the Nag Library, which calculates the smoothed sample spectrum of a univariate time series using spectral smoothing by the trapezium frequency (Daniell) window (Numerical Algorithms Group 1984).

c. *Return maps*

The return map has been introduced above in the discussion of the circle map and may be extended for any system undergoing the quasi-periodicity route to chaos as follows. The model time series is embedded in a two-dimensional phase space using the delay coordinates described above. The phase space trajectory of a quasi-periodic system lies on a two-dimensional torus (the combination of two independent frequencies). A section through this torus obtained by the annual subsampling of the time series used in the phase space reconstruction results in a simple closed curve in phase space. An angle θ_n is then defined from a point $(h(t_n), h(t_n + \tau))$ in phase space that is on this closed curve (Fig. 3). Calculating θ_n from this phase space picture, we can obtain the return map numerically by plotting θ_{n+1} versus θ_n.

d. *Histograms of ENSO events distribution*

Apart from the above commonly used diagnostics for examining the behavior of chaotic systems, we found two additional diagnostics to be most useful for analyzing the ENSO model time series. The first is a histogram of the number of ENSO events per month of the calendar year. This simple diagnostic provides a measure of the locking to the seasonal cycle of the ENSO model at a given parameter regime. The second diagnostic is a histogram of the distribution of separation between events. That is, we examine the time separation between adjacent model ENSO events and count the number of occurrences of a separation of, say, 4 years. The resolution of this histogram was chosen to be 3 months. The use of this diagnostic will become more apparent in the following.

For both of these diagnostics, an ENSO "event" is defined to be a local maximum in the time series over a period of 3 years (i.e., 1.5 years before and 1.5 after the event). Restricting events to be of a some minimum amplitude did not seem to change the results significantly. In addition, we have not examined the model time series directly, but only the 12 months running average of the time series. This eliminates the seasonal cycle from the data, leaving only the interannual signal. Note that although the CZ model is a perturbation model for variations from the monthly climatology, the model nonlinearity rectifies the seasonal background fields so that the perturbation model fields have a nonvanishing monthly mean seasonal cycle (Fig. 4). This model seasonal cycle, when superimposed on the interannual variability, may create artificial peaks in the time series, and in particular shift the month at which a given interannual peak occurs. The simple running average seems to efficiently eliminate this problem. The 12-month running average acts as a low-pass filter but does not change the number of NINO3 time points per year, so that it is still possible to use the resolution of 3 months in the histograms discussed above.

5. Transition to chaos of the CZ model

We now describe a set of experiments in which either the strength of the background seasonality or the drag coefficient is varied and examine the model behavior as function of these parameters. A summary of all the experiments is given in Table 1.

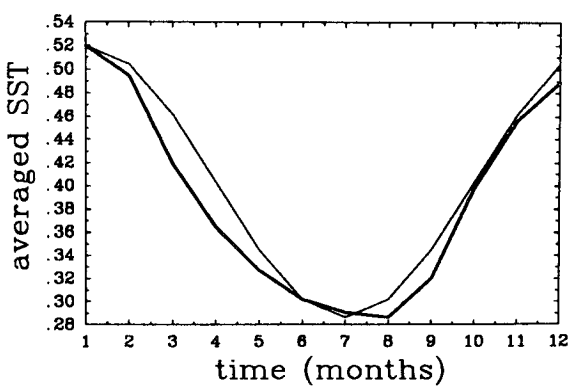

FIG. 4. Monthly averaged East Pacific SST (degrees Celsius) from a 1024-year run of the Cane–Zebiak model (thick line), and a fitted cosine function with a one-year period (thin line).

TABLE 1. Summary of model runs used in this study.

Run	Drag coeff. r_d	Seasonality a_{seasonal}	Model state	Comments	Figure
a1	1.0	1.0	chaotic	standard run	5
a2	0.8	1.0	mode locked		6
a3	0.9	1.0	chaotic		7
b	1.0	0.0	zero state	annual avg	—
c	1.0	0.0	chaotic	perpet. July	8
d1	0.9	0.0	periodic	perpet. July	9
d2	0.9	0.2	mode locked		10
d3	0.9	1.0	chaotic	same as a3	7

a. Varying the drag coefficient

As explained above, the drag coefficient is one of the factors determining the coupling strength between the ocean and the atmosphere in this model. Therefore, following T94 in which an effective coupling strength parameter was varied in the simple delay model, we begin our experiments by varying the drag coefficient r_d in the CZ model.

Consider first the model run we consider "standard" (run a1) with an unreduced drag coefficient. A similar run was analyzed in T94 and was found to be consistent with low-order chaotic behavior of the model. The present analysis of the NINO3 time series from this standard model run is shown in Fig. 5. This model state is aperiodic (Fig. 5a), characterized by a wide spectrum (Fig. 5b), with evidential partial locking to the seasonal cycle (Fig. 5e).

In the next experiment, the relative drag coefficient is reduced from 1.0 to 0.8 (run a2, Fig. 6). In this case the model NINO3 time series is very regular once all initial transients have dissipated. The spectrum has a sharp main peak at $1/4\ \text{yr}^{-1}$ (plus many subharmonics due to the model nonlinearity), and the reconstructed phase space structure is simply four dots with some scatter around each of them. This is clearly a solution that is mode locked to the seasonal cycle at a 1 to 4 nonlinear resonance. The histograms also indicate that this is a mode-locked state: the distance between peaks is always 4 years, and the peaks always occur at the same two months of the calendar year. It is important to emphasize that the mode-locked parameter regime does not consist of a single value of the drag coefficient resulting in this behavior but extends over a significant range of this parameter.

Further decreasing the drag coefficient leads to the elimination of the ENSO oscillations in the model. The model solution for the perturbations to the background state are zero at all times (again, after initial transients have dissipated).

The above picture is very satisfying, showing that the CZ model behavior is, in fact, consistent with the quasi-periodicity route to chaos: as the effective model nonlinearity (now measured by the r_d) is increased, the model is first mode locked and then aperiodic. Additional experiments show that the degree of aperiodicity depends on the value of the drag coefficient; an intermediate value between the model standard solution and the mode-locked solution is shown in run a3 of Table 1 and in Fig. 7.

Clearly we have not exhausted the entire parameter regime, and there are many more interesting experiments that can be envisioned, such as taking finer steps in parameter space of further increasing the drag coefficient beyond $r_d = 1$. In any case, the experiments shown here seem to be more than sufficient to establish the transition to chaos scenario in the model, so we may now refer to the aperiodicity regime in the CZ model as chaos. We further strengthen this case by showing that varying the amplitude of the background seasonality results in the same route to chaos.

b. Varying the background seasonality

The relevant runs in Table 1 are now b, c, d1, d2, and d3. Our purpose in this set of runs was to find a more complete quasi-periodicity route to chaos that contains not only the mode-locked and chaotic regimes, but also the periodic or quasi-periodic regime that is neither mode locked nor chaotic (see discussion of the circle map in above section and T94). While looking for a complete transition scenario, we will also learn more about the factors leading to aperiodicity in the CZ model.

We begin by setting the seasonality amplitude [a_{seasonal} in (4)] to zero, looking for the natural oscillatory mode of the model ENSO system that is not forced by the seasonal cycle. The first attempt is run b, in which all background model fields were set to their annual mean values [$\bar{F}_{i,j}^{\text{data}} = \sum_{l=1}^{12} F_{i,j,l}^{\text{data}}/12$ in (4)]. Unfortunately, this background state does not seem to be sufficient to support any ENSO oscillations, and the model solution vanishes after transients are dissipated.

Noting that Zebiak and Cane (1987) found July to be the most unstable month in their simulations, we next try to set all background fields to their July value ($\bar{F}_{i,j}^{\text{data}} = F_{i,j,7}^{\text{data}}$; run c, Fig. 8). This run turns out to be very interesting: the model time series is characterized by ENSO events that are irregular, seemingly chaotic. This is quite surprising as we anticipated that the reason for the chaotic behavior in this model is the periodic (seasonal) forcing, and that is completely missing in this run. Evidently, the model nonlinearity is sufficient to cause aperiodic behavior even in the absence of seasonal forcing. Note (Fig. 8e) that the distribution of ENSO events is no longer locked to the seasonal cycle (which is now absent in the model); rather, they occur all over the calendar year.

We proceed to run d1, in which all background model fields have been set to their July values, as in run c, but this time the drag coefficient is also reduced to 0.9. This finally results in regular periodic ENSO events (Fig. 9) with a frequency that is not a simple

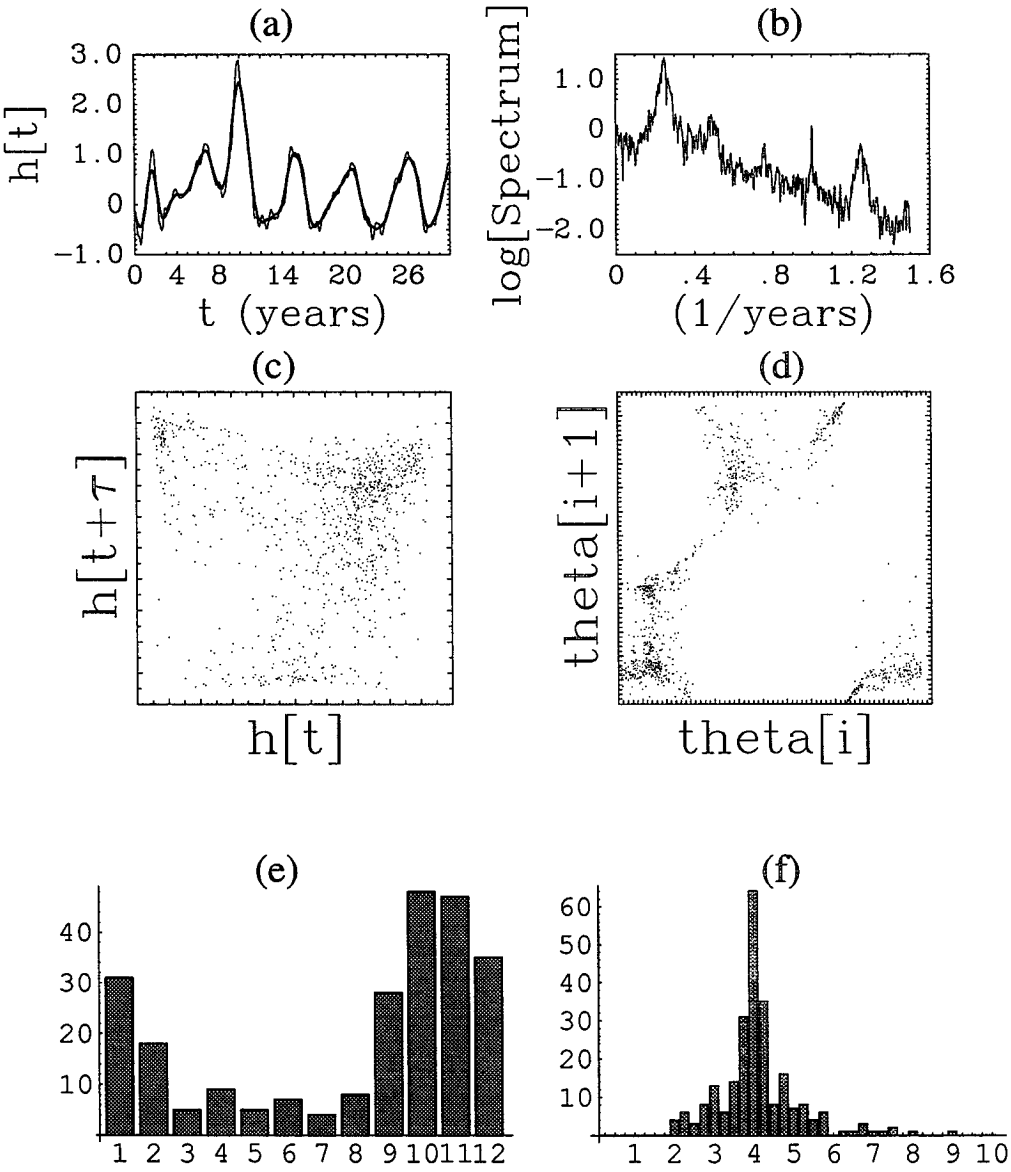

FIG. 5. Run a1: the standard case. Shown are various analyses of the model NINO3 index time series; see section 4 for more details. (a) A 30-year portion of the model time series being analyzed. Shown are the actual monthly NINO3 index from the model (thin line) and its 12-month running average (thick line). (b) The power spectrum of the model time series. (c) The reconstructed phase space picture. (d) Return map plotted from the time series. (e) A histogram of the number of ENSO events (vertical axis) per month of the calendar year (horizontal axis). (f) A histogram of the distribution of separation between model ENSO events. Horizontal axis: separation between events in years; vertical axis: number of times a given separation is seen in the time series. See section 4d for details concerning (e) and (f).

integer ratio of the annual frequency. The events are spread all over the calendar year, with separation of about 4.25 years between events. The power spectrum has a sharp peak at this frequency, with many subharmonics seen as well. This run is the starting point for the route to chaos we now follow. This run also seems to be in the same regime as the one run by Zebiak and Cane (1987) with perpetual July conditions. They have used a full-strength drag coefficient but a slightly different algorithm for computing the atmospheric heating, amounting to a weaker coupling strength, and also found a periodic solution (see their Fig. 18).

The next run (d2) has the amplitude of the background seasonality increased to 0.2 while keeping $r_d = 0.9$. Because $\vec{F}_{i,j}^{\text{data}}$ in (4) is set to the July climatology, the model background fields are now a weighted

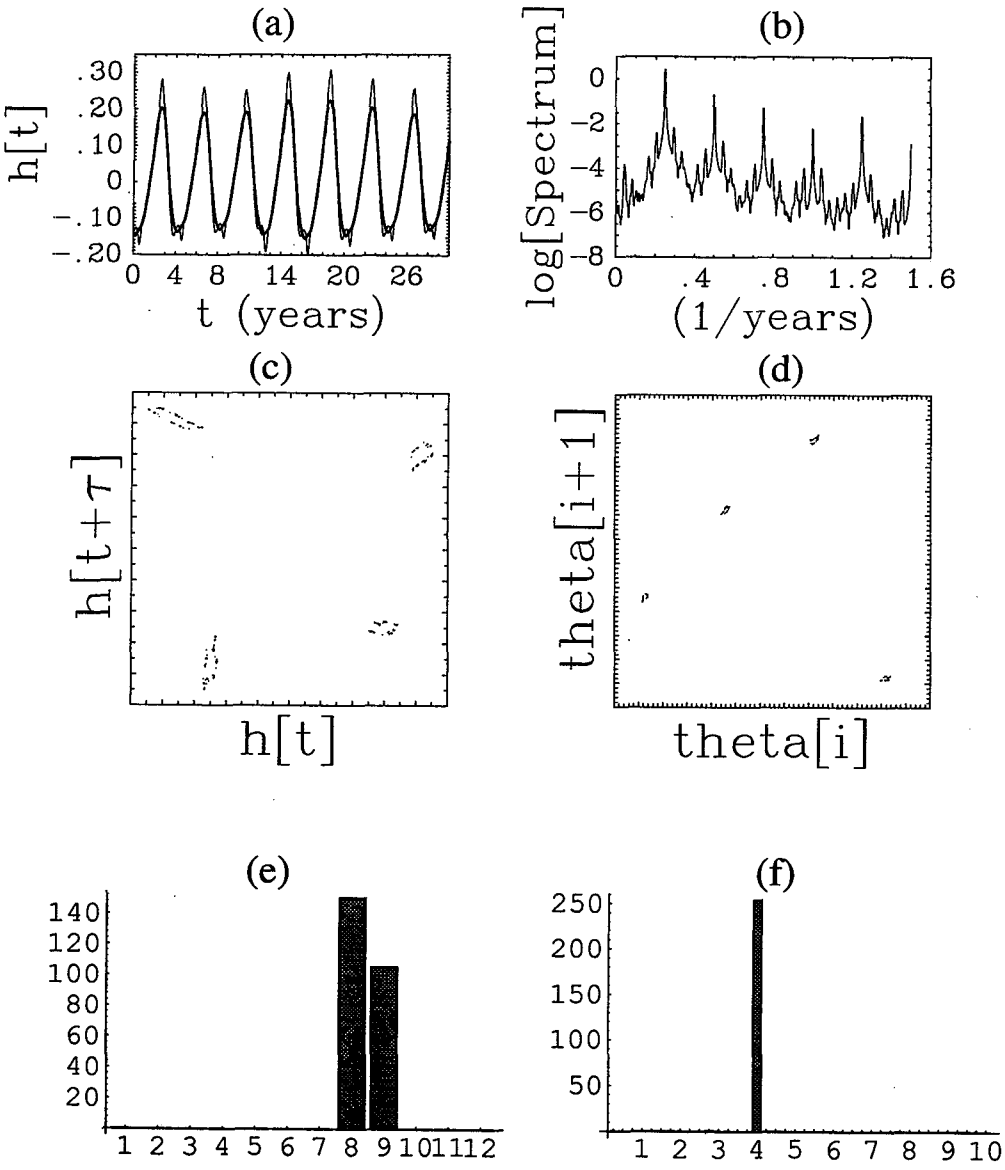

FIG. 6. Run a2. Mode-locked solution using fully seasonal model background with relative drag coefficient reduced to 0.8 (see caption of Fig. 5).

average of the July climatology and the fully seasonal climatology. At this point the model is again mode locked (Fig. 10). Further increasing the seasonality to 1.0 (run d3, which is identical to run a3; Fig. 7) results in chaotic behavior, as expected from the quasi-periodicity route to chaos scenario. Note, however, that the ENSO events at this parameter setting ($r_d = 0.9$) are less irregular than in the standard model run (compare Figs. 5a and 7a) as is the spacing between events (compare Figs. 5f and 7f). Increasing the drag coefficient from 0.9 to 1.0 restores the parameter regime of the standard model run with its fully chaotic behavior.

c. *Discussion*

The above numerical experiments have confirmed that the basic characteristics of the CZ model ENSO events are dominated by a low-order chaotic behavior driven by the seasonal cycle and consistent with the universal properties of the quasi-periodicity route to chaos.

This explanation clearly accounts for the model ENSO's irregularity, but how does it explain the partial locking to the seasonal cycle? Note that each of the main nonlinear resonances, that is, those with a winding number of $1/Q$ where Q is an integer, corresponds

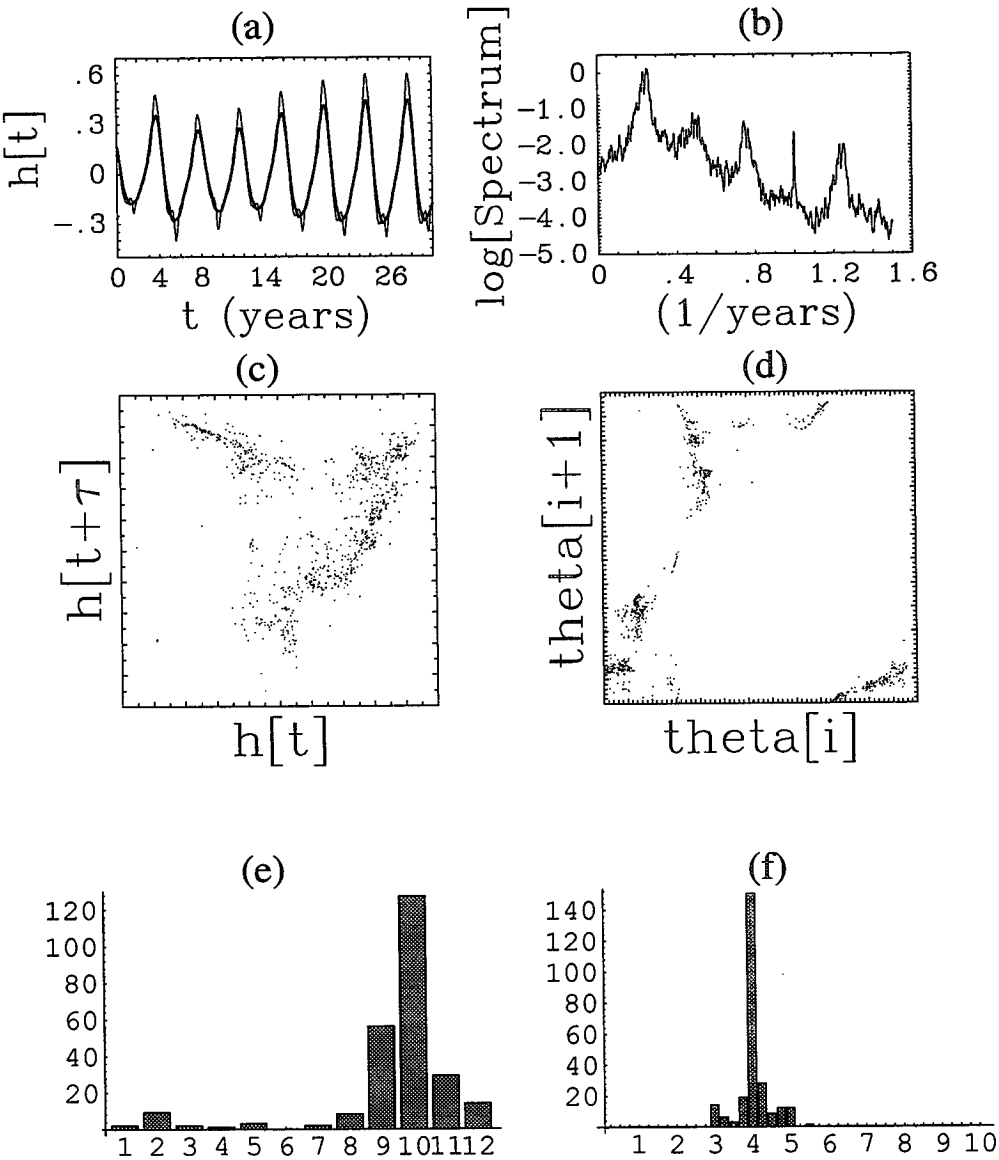

FIG. 7. Run a3. Chaotic solution using fully seasonal model background with relative drag coefficient reduced to 0.9 (see caption of Fig. 5).

to a perfectly periodic solution of a period of exactly Q years. The ENSO events in this parameter regime will occur, of course, always at the same month of the calendar year. When two or more of these main resonances overlap and the system irregularly jumps between them, the ENSO cycle could be thought of as spending several years at a given resonance, then jumping to another, etc. Because each of these resonances is locked to the seasonal cycle, the ENSO events in the chaotic regime still tend to be locked to the seasonal cycle, although only partially now, due to the inability of the system to remain at a given resonance for a long time.

But this explanation ignores the secondary resonances. These are the resonances with winding number P/Q with both P and Q being integers, such as 2/3, 2/5, 3/5, etc. Note that a resonance such as 2/5 will have ENSO events every 2.5 years. As a result, these events will occur in two distinct parts of the calendar year, separated by 6 months. Thus, the system seems to lose its locking to the seasonal cycle when these secondary resonances dominate the solution. When even higher-order resonances are considered (e.g., 7/15), the locking to the seasonal cycle is even further degraded. We have clearly seen that the ENSO events in the chaotic regime of the CZ model (as well as in

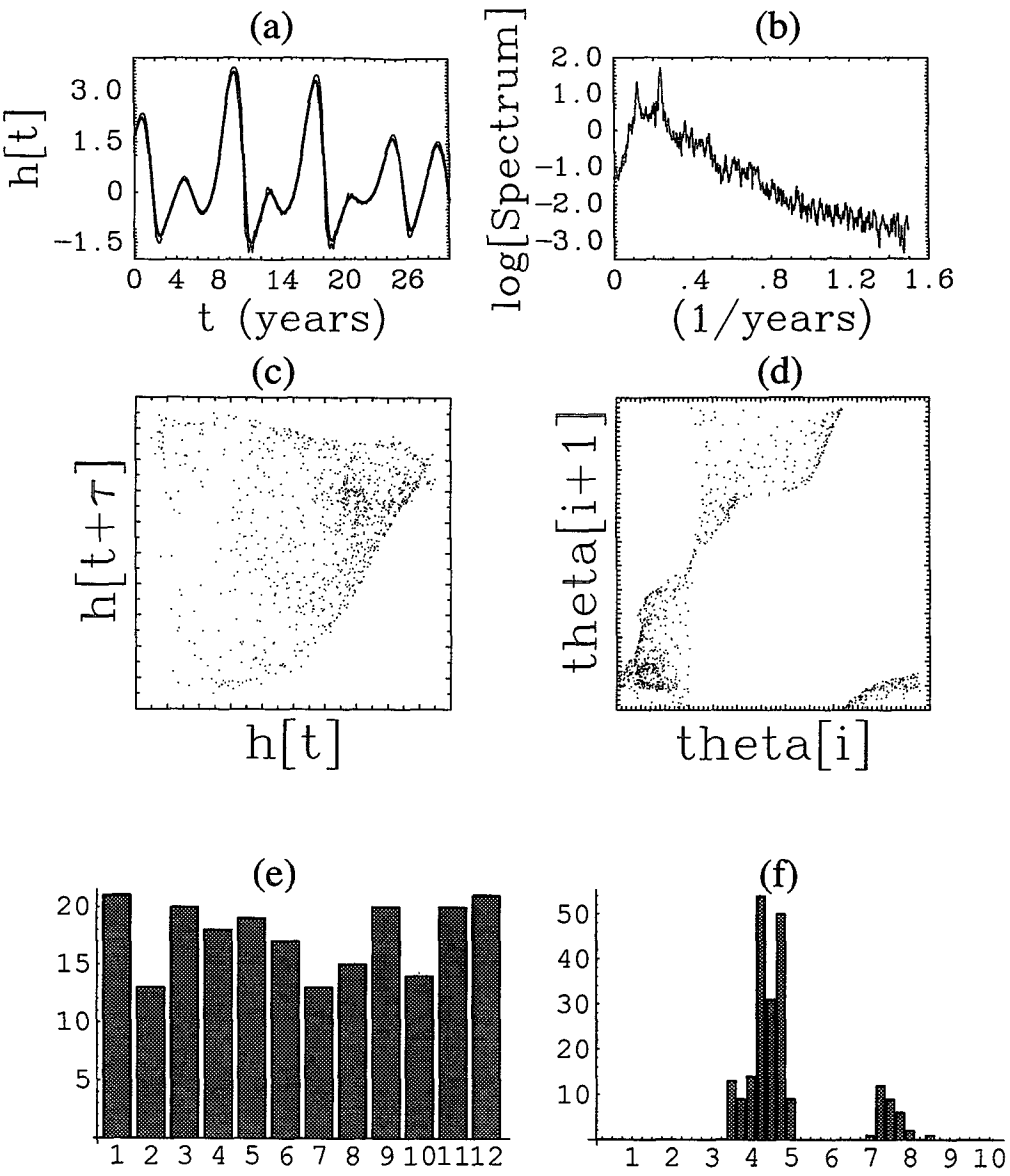

FIG. 8. Run c. Aperiodic solution using perpetual July model background with the relative drag coefficient set to its standard value of 1.0 (see caption of Fig. 5).

the simple delay model of T94) do tend to be locked to the seasonal cycle. This leads to the conclusion that the secondary resonances do not dominate the solution. But why? We cannot offer a complete answer but can provide two alternative explanations for the weaker influence of the secondary resonances between the ENSO cycle and the seasonal cycle.

The first explanation is simply that the secondary resonances are weaker than the main ones for the following reason: ENSO events in the nonlinear resonance 7/2, for example, happen every 3.5 years. Assume, for example, that the events occur in January and July. Presumably, the seasonal cycle is such that it forces the ENSO events in the right way in only one of these two months. This means that the ENSO events in the 7/2 resonance are forced only every second event, that is, every 7 years. Clearly, such a resonance will be weaker than 1/3 or 1/4, which are forced every event, that is, every 3 or 4 years.

A second possible explanation for the dominance of the main resonances may be that the secondary resonances are less stable than the main ones in the chaotic regime. In the chaotic regime all resonances (i.e., mode-locked solutions) are clearly unstable, as the system does not remain at any of them for too long. But consider the possibility that the secondary resonances

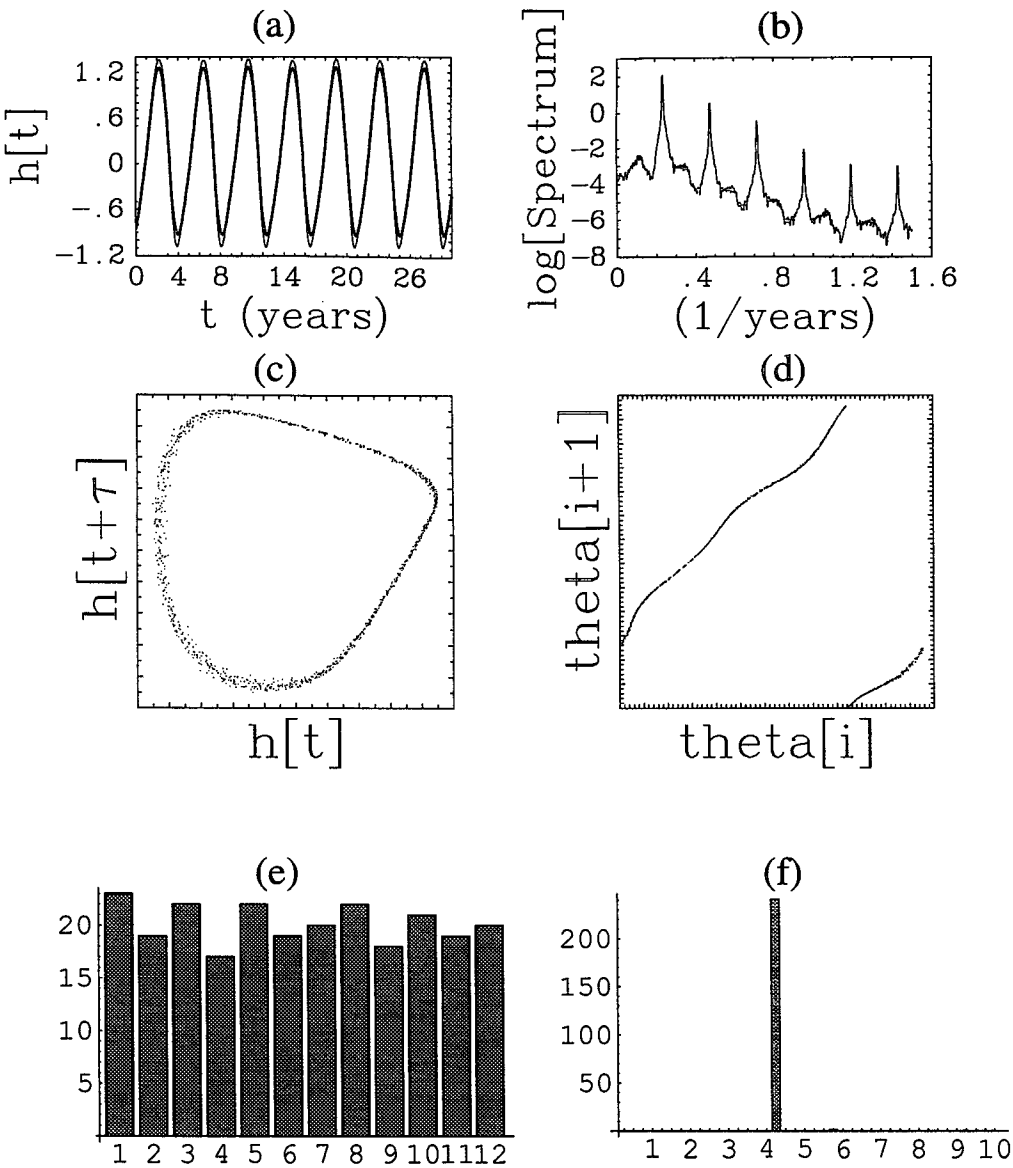

FIG. 9. Run d1. Quasi-periodic regime; solution obtained using perpetual July model background with the relative drag coefficient set to 0.9 (see caption of Fig. 5).

are less stable than the main ones. Then, even if the ENSO system happens to be trapped by one of the secondary resonances for some time, it will leave this resonance much faster than it would leave a main resonance.

Distinguishing between the two explanations would require nontrivial mathematical analysis we leave to future work. For the present, we simply note the empirical evidence that the main resonances between ENSO and the seasonal cycle are more dominant in the chaotic regime, which results in the observed locking of model ENSO events to the seasonal cycle.

While the quasi-periodicity route to chaos seems to be able to provide an attractive explanation for ENSO's irregularity and locking to the seasonal cycle, there are some additional observations we can make based on our experiments. The most interesting observation is that the explanation of the fully chaotic behavior of the CZ model requires, in fact, more than the forcing by the seasonal cycle. This was seen in two of the above experiments: First, run c, when the model background state is a perpetual July state and the drag coefficient is set to its standard value, the model solution is aperiodic in spite of the absence of the background seasonality. Some aspects of the background seasonal cycle are still important, as the annual average background run resulted in a zero solution (run b). Still, this aperiodic solution is not explicitly forced by a pe-

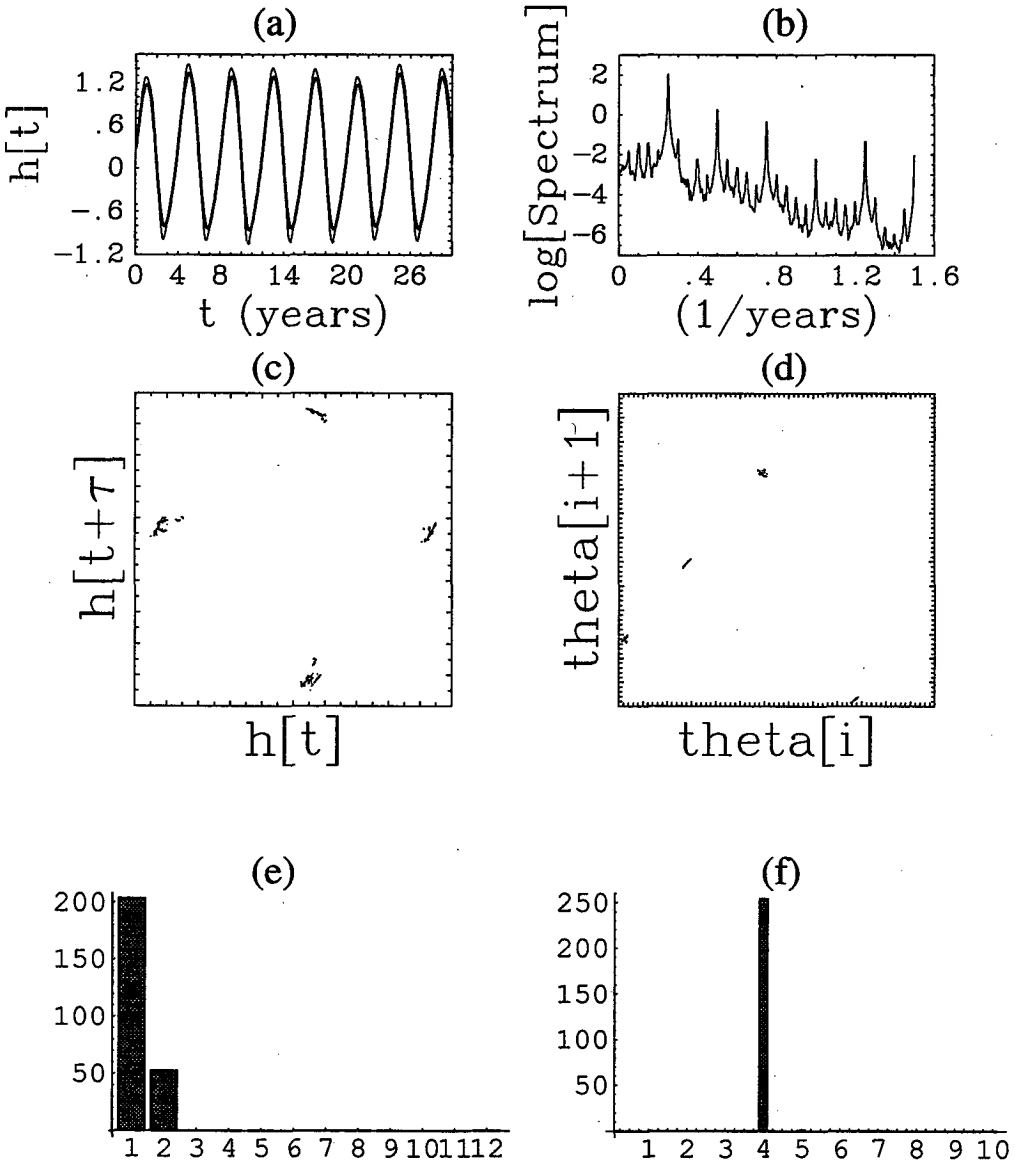

FIG. 10. Run d2. Mode-locked regime; solution obtained using model background seasonality amplitude of 0.2 with the relative drag coefficient set to 0.9 (see caption of Fig. 5).

riodic seasonal forcing as implied by the quasi-periodicity scenario.

The second occasion in which the basic quasi-periodicity scenario seems to be an incomplete explanation for ENSO's behavior (at least in this model) is in runs d1–d3. Increasing the seasonal forcing in these runs resulted in a transition from periodic to mode-locked to chaotic regimes, yet the final chaotic regime (run d3) did not seem sufficiently irregular in terms of both amplitude and separation of model ENSO events until the drag coefficient was raised to its standard value (run a1). It seems that while the seasonal forcing is a major contributor to the model's irregularity, the model nonlinearity can result in irregular behavior without the seasonal forcing and can supplement the chaos mechanism due to the seasonal forcing. Note that the seasonal forcing mechanism also requires the model to be nonlinear in order to allow for chaotic behavior.

These observations reinforce the findings of Munnich et al. (1991), who showed that a simple delay model with more than a single Rossby wave may result in chaotic behavior even in the absence of seasonal forcing. It seems that the nonlinear interaction of the different possible delay oscillators due to the different Rossby modes included in the model is capable of amplifying the chaotic mechanism due to the seasonal

forcing. Munnich et al. (1991) have also shown that when an annual forcing is included in their model (through a seasonal dependence of a parameter roughly representing the coupling strength between the ocean and atmosphere), their delay model behavior is made irregular much more easily. This observation may now be understood to be a direct result of the seasonally driven chaos mechanism given in T94 and Jin et al. (1994).

6. Conclusions

We have examined the hypothesis that the irregularity of ENSO events in the CZ model and their partial locking to the seasonal cycle may be explained as low-order chaotic behavior driven by the seasonal cycle. We have varied model parameters that determine the strength of the seasonal cycle and the strength of the coupling between the ocean and atmosphere in the CZ model and examined the model behavior as a function of these parameters. The analysis of the model transition to chaos as a function of these parameters results in a clear demonstration that the basic behavior of the CZ model is most probably dominated by low-order chaos.

An important conclusion of this study concerns the chaos mechanism in the CZ model. This mechanism seems to be chiefly due to the forcing by the seasonal cycle as suggested by Tziperman et al. (1994) and by Jin et al. (1994): the natural oscillator of the equatorial Pacific coupled ocean–atmosphere system can enter into nonlinear resonance with the seasonal cycle at several periods of the oscillator (mostly 3–5 years). The coexistence of these resonances results in chaotic behavior due to the irregular jumping of the system between the different resonances. The behavior of the CZ model as the above parameters are changed is consistent with the universal properties of the quasi-periodicity route to chaos (BBJ84). This route to chaos implies that a nonlinear oscillator may become chaotic due to periodic forcing. It seems that this route to chaos is shared by other models as well, as recently reported by Chang et al. (1994), using a different coupled ocean–atmosphere model.

We found here that the nonlinearities in the CZ model seem to be sufficient to support chaotic behavior even without the periodic seasonal forcing. When both the periodic forcing and the fully coupled dynamics (i.e., relative drag coefficient equal to 1 in our experiments) are present, the model irregularity is enhanced as compared to that due to the periodic forcing alone or the fully coupled case without the seasonal forcing. Following Munnich et al. (1991), we suggest that the enhancement of the chaos mechanism by model nonlinearity may be partially explained by the nonlinear interaction of different delay oscillator modes that correspond to the many Rossby modes existing in the CZ model.

The careful reader has no doubt noticed that no claims have been made here about the actual ENSO system. This work has been offered as an explanation of the irregular behavior of the CZ model only. Of course, we do feel that our findings are relevant to the behavior of the coupled Pacific ocean–atmosphere system because we have some confidence that the model captures the principal physics of the real world ENSO. However, a more definite demonstration that low-order chaos and not random noise is responsible for the actual ENSO variability may require experimentation with models that also include random noise due to atmospheric weather. Obviously, it would be more satisfying to work directly with observations of ENSO and show that they bore the signature of a low-order chaotic system following the quasi-periodic route. However, we have little more than 100 years of instrumental data, and it is well known that this is far too short a record to unequivocally distinguish between low-order chaos and random noise by any of the standard dynamical systems techniques for analyzing time series (e.g., Eckmann and Ruelle 1992).

While this work is a further step toward a fuller understanding of ENSO chaos as compared to the simpler models of Tziperman et al. (1994), Jin et al. (1994), and Munnich et al. (1991), our understanding of the chaos mechanism is still incomplete. What is needed now is a better understanding of the spatial and temporal physical mechanisms of chaos from further model studies. In particular, one would like to know which of the seasonal fields (i.e., ocean upwelling, winds over the ocean, etc.) is the major forcing of the nonlinear resonances and therefore of the chaotic behavior in the model. A better structural description can then be tested against the richer array of ENSO observations available only for recent decades.

Acknowledgments. We thank Larry Rosen for his help, and three anonymous reviewers for especially constructive comments. This work was done during a visit of ET to the Geophysical Fluid Dynamics Laboratory in Princeton University, for whose hospitality we are grateful. This work is partially supported by a grant from NOAA through the Consortium for Climate Research, UCSIOPO-10775411D/ NA47GP0188. SZ and MC are supported by a NOAA grant and by NSF Grant ATM92-24915.

REFERENCES

Bak, P., T. Bohr, and M. H. Jensen, 1985: Mode-locking and the transition to chaos in dissipative systems. *Physica Scripta,* **T9,** 50–58.

Battisti, D. S., and A. C. Hirst, 1989: Interannual variability in the tropical atmosphere/ocean system: Influence of the basic state, ocean geometry and nonlinearity. *J. Atmos. Sci.,* **46,** 1687–1712.

Bohr, T., P. Bak, and M. H. Jensen, 1984: Transition to chaos by interaction of resonances in dissipative systems. II. Josephson junctions, charge-density waves, and standard maps. *Phys. Rev. A,* **30,** 1970–1981.

Cane, M. A., M. Munnich, and S. E. Zebiak, 1990: A study of self-excited oscillations of the tropical ocean–atmosphere system. Part I: Linear analysis. *J. Atmos. Sci.,* **47,** 1562–1577.

Chang, P., B. Wang, T. Li, and L. Ji, 1994: Interactions between the seasonal cycle and the southern oscillation—Frequency entrainment and chaos in a coupled ocean–atmosphere model. *Geophys. Res. Lett.,* **21**(25), 2817–2820.

Eckmann, J.-P., and D. Ruelle, 1992: Fundamental limitations for estimating dimensions and Lyapunov exponents in dynamical systems. *Physica D,* **56,** 185–187.

Fraser, A. M., and H. L. Swinney, 1986: Independent coordinates for strange attractors from mutual information. *Phys. Rev. A,* **33,** 1134–1140.

Graham, N. E., and W. B. White, 1988: The El Niño cycle: A natural oscillator of the Pacific ocean–atmosphere system. *Science,* **240,** 1293–1302.

Grassberger, P., and I. Procaccia, 1983: Measuring the strangeness of strange attractors. *Physica D,* **9,** 189.

Jensen, M. H., P. Bak, and T. Bohr, 1984: Transition to chaos by interaction of resonances in dissipative systems. I. Circle maps. *Phys. Rev. A,* **30,** 1960–1969.

Jin, F.-F., D. Neelin, and M. Ghil, 1994: ENSO on the devil's staircase. *Science,* **264,** 70–72.

Munnich, M., M. A. Cane, and S. E. Zebiak, 1991: A study of self-excited oscillations of the tropical ocean–atmosphere system. Part II: Nonlinear cases. *J. Atmos. Sci.,* **48,** 1238–1248.

Neelin, J. D., M. Latif, and F.-F. Jin, 1994: Dynamics of coupled ocean–atmosphere models: The tropical problem. *Ann. Rev. Fluid Mech.,* **26,** 617–659.

Numerical Algorithms Group, 1984: *Fortran Library Manual, Mark II,* 6 vols.

Philander, S. G., 1990: *El Niño, La Niña, and the Southern Oscillations.* Academic Press,

Rasmusson, E., and T. Carpenter, 1982: Variations in the tropical sea surface temperature and surface wind fields associated the Southern Oscillations/El Niño. *Mon. Wea. Rev.,* **110,** 354–384.

Suarez, M. J., and P. S. Schopf, 1988: A delayed action oscillator for ENSO. *J. Atmos. Sci.,* **45,** 3283–3287.

Tziperman, E., L. Stone, M. Cane, and H. Jarosh, 1994: El Niño chaos: Overlapping of resonances between the seasonal cycle and the Pacific ocean–atmosphere oscillator. *Science,* **264,** 72–74.

Vallis, G. K., 1986: El Niño: A chaotic dynamical system? *Science,* **232,** 243–245.

——, 1988: Conceptual models of El Niño and the Southern Oscillations. *J. Geophys. Res.,* **93C,** 13 979–13 991.

Zebiak, S. E., and M. Cane, 1987: A model El Niño–Southern Oscillation. *Mon. Wea. Rev.,* **115,** 2262–2278.